Investigation of a Complex Reaction Network: II. Kinetics, Mechanism and Parameter Estimation

Y. Jiang, M. R. Khadilkar, M. Al-Dahhan, and M. P. Duduković
Chemical Reaction Engineering Laboratory (CREL), Dept. of Chemical Engineering, Washington University, St. Louis, MO 63130

S. K. Chou, G. Ahmed, and R. Kahney
The Agricultural Group, Monsanto Company, St. Louis, MO 63167

Conventional strategies for discrimination of intrinsic and apparent kinetics from crushed- and whole-catalyst-pellet experimental data, respectively, do not yield satisfactory results for the reaction network in the manufacture of α-aminomethyl-2-furanmethanol (aminoalcohol) from α-nitromethyl-2-furanmethanol (nitroalcohol). Laboratory trickle-bed reactor tests in the range of concentration and product yield of commercial interest are utilized to yield a reasonable set of kinetic parameters, which are otherwise unobtainable. This is accomplished by proposing a reaction network, a plausible mechanism, and optimizing the kinetic parameters based on the reactor-model-generated performance data to fit experimental output concentrations of all species for the entire set of experiments. A complex reaction network for the key reactions in the system is developed based on the reaction scheme in Part I. Fitting of trickle-bed reactor data to this model is attempted to yield an insight into the actual kinetics. The results show promise of obtaining an overall network kinetic model, even with the limited data available.

Introduction

A feasibility study aimed at achieving high productivity and selectivity for manufacturing aminoalcohol (AA) from nitroalcohol (NA) in a trickle-bed reactor was presented in Part I. The superiority of trickle-bed reactors over other reactor configurations such as semibatch and batch slurry systems was also demonstrated. The sequence of steps often suggested in trickle-bed scale-up and performance evaluation studies is to obtain the catalyst activity and intrinsic kinetics from slurry reactions using powdered catalyst followed by generating the apparent kinetics using the actual catalyst particles enclosed in a wire-mesh basket under fully wetted conditions (Beaudry et al., 1987). These yield the intrinsic and the apparent kinetics of the catalyst for a given reaction system, which can then be tested in a trickle-bed reactor to get the information necessary for scale-up, design, and performance evaluation.

The complexity of the reactions in the reaction system presented prevents product formation at low catalyst-to-liquid volume ratios. When the activity of the catalyst is low and the catalyst-to-liquid volume ratio is low, the reactant NA decomposes homogeneously to furfural (F) and nitromethane (NM). The product AA catalyzes this decomposition (refer to Figure 1 of Part I). When this occurs, byproducts nitrone (NR) and reduced nitrone (RN) are produced from the reaction of F with the intermediate B and product AA, respectively. These byproducts can in turn be slowly converted back to the desired product AA. Therefore, the catalyst activity is the critical issue in achieving high conversion and selectivity. A catalyst of high activity would convert the entire reactant to the desired product before any decomposition (and byproduct formation) can take place. Unfortunately, we cannot get any intrinsic kinetic data due to the special characteristics of this complex reaction system where a significant drop in yield occurs in batch and semibatch conditions at high reactant feed concentrations, as discussed below. The trickle-bed reactor experiments are thus important and utilized in a threefold

Correspondence concerning this article should be addressed to M. Al-Dahhan.

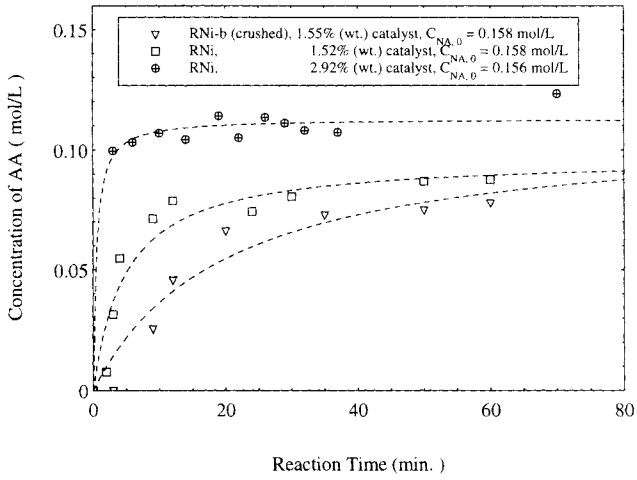

Figure 1. Comparison of powdered (RNi) and crushed (RNi-b) catalyst activity in a slurry reactor.

purpose: (1) to test feasibility as opposed to other configurations; (2) to obtain conversion and selectivity levels desired for commercial reactors; and (3) to get kinetic information in the desired range of concentrations of all relevant species. In order to obtain the kinetic parameters, it was necessary to propose a suitable network in which all species could be quantitatively analyzed. A plausible reaction mechanism is required, since most of these are heterogeneous reactions and mass action can be applied to only homogeneous steps. A reactor model, which is simple and still captures the essential features, is also needed. These are proposed, and results based on model fitting of the trickle-bed data are presented.

Experimental Tests for Kinetic-Parameter Determination

As mentioned in Part I, in order to obtain the apparent (particle) kinetics, the catalyst, RNi-b (mean size 2.6 mm), was tested in a fixed-basket reactor for activity at catalyst loading ranging from 12 to 29 wt. % and initial reactant concentrations ranging from 1 to 10 wt. %. It was found (Table 1, runs 4 and 5) that the catalyst particles did not produce any yield (i.e., any AA product) even after one hour of reaction time. The same observation was obtained when the catalyst loading was increased from 40 g (Table 1, runs 4 and 5) to 87.1 g (Table 1, run 6) without using the basket. In order to examine whether some activity can be obtained when the intraparticle diffusional resistance is reduced, the same catalyst (RNi-b) was crushed (under water) into powder (mean size $\sim 40\ \mu$m), and the reaction was run at low initial reactant concentrations. It was observed that the desired product is indeed produced (Table 1, run 6). However, the activity (and yield) was below that of the powder catalyst of comparable size (RNi) (Figure 1). It must be noted that the yield obtained in either case (Figure 1) was also low (about 50%). The preceding observations indicate that the activity of the internal area of RNi-b catalyst is lower than that required to obtain meaningful intrinsic kinetics. Typical methods of preparation of Raney Nickel catalyst also do not distribute activity equally into the interior of the catalyst, which when crushed (as done for RNi-b) does not increase the activity to the same extent of the powdered catalyst (RNi). Thus, no intrinsic or apparent rate data determination was possible from this experimentation. This situation can arise in many complex reaction systems where intrinsic and apparent rate data may not be obtainable in a stirred vessel in the desired range of concentration yields and product yield. This necessitated proposing a reaction network to obtain kinetic parameters based on trickle-bed reactor performance data.

Reaction Network, Mechanism, and Kinetics

The reaction scheme investigated in this study contains several side reactions as presented in Figure 1 of Part I, for which the amount of products formed is not significant enough or not detectable by the present analytical method. Most of the secondary byproduct species are not produced in significant amounts when the yield of the main reaction is 50% or higher. In order to obtain any kinetic model fit with the limited data available, the network of reactions must be simplified to reflect only the main reaction and some of the side reactions, involving those species, which are amenable to quantitative analysis. This was done to develop the proposed reaction network, which is represented below:

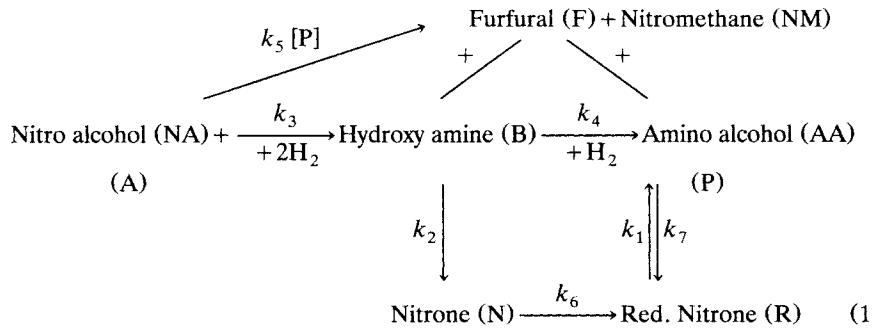

The reactions represented here (except the decomposition of the reactant NA to F and NM) are assumed to be heterogeneous, and governed by typical Langmuir–Hinshelwood type of kinetics, which is characterized by adsorption of the reactants on the active sites of the catalyst (represented by σ in the mechanism below) followed by surface reaction and desorption of the products back into the liquid. Hydrogen is assumed to remain unadsorbed (for the sake of model sim-

Table 1. Operating Conditions for Batch Experiments

Exp. No.	Catalyst	Catalyst mass (g)	C_{cat} (wt. %)	$C_{0,NA}$ (wt. %)	$C_{0,NA}$ (mol/L)	Max. Yield(%)
Run 1	RNi powder	9.00 Slurry	2.915	3.732	0.1563	71.0
Run 2	RNi powder	4.68 Slurry	1.520	3.672	0.1577	55.2
Run 3	RNi-b crushed	4.81 Slurry	1.550	3.763	0.1582	49.3
Run 4	RNi-b particles	40.0 Basket	12.62	9.46	0.3974	0
Run 5	RNi-b particles	40.0 Basket	13.14	1.025	0.0431	0
Run 6	RNi-b particles	87.1 No basket	28.68	0.995	0.0418	0
Run 7	RNi-b particles	48.0 Semibatch	87.59	27.31	1.248	0

plicity) on the active sites and to react directly with other adsorbed species via an Ely–Rideal-type mechanism. Another assumption in obtaining the rate forms is that the adsorption and desorption are instantaneous (reach equilibrium much faster) as compared to surface reactions, which are considered to be the rate-controlling steps of each individual reaction. Since the relative magnitudes of the rates of the individual surface reactions in the network are not known accurately, no assumption is made regarding an overall rate-controlling surface reaction. The homogeneous reaction (decomposition of reactant, NA to F and NM) rate is formulated by the law of mass action, with the products being released into the bulk liquid without any adsorption on catalyst sites. It is also assumed that the same types of active sites are responsible for all the reactions with only monosite adsorption possible. Based on these assumptions, a reaction mechanism can be postulated as follows (note that the numbering of the rate equations presented here differs from the final numbering in terms of the seven rate constants as given in the processed reaction network (Eq. 1):

1. Surface Reaction Steps with Corresponding Rate Equations. ($A\cdot\sigma$, $B\cdot\sigma$, etc. are adsorbed species with concentrations $(A\cdot\sigma)$, $(B\cdot\sigma)$, etc., which are eliminated using adsorption/desorption equilibrium relations (Eqs. 8–12)).

$$A\cdot\sigma + 2H_2 \xrightarrow{m_2} B\cdot\sigma + (H_2O)$$

$$\Rightarrow r_2 = m_2(A\cdot\sigma)C_{H_2}^2 = m_2 M_1 C_A C_{H_2}^2 \sigma_V \quad (2)$$

$$B\cdot\sigma + F \xrightarrow{m_3} N\cdot\sigma$$

$$\Rightarrow r_3 = m_3(B\cdot\sigma)C_F = \frac{m_3}{M_{10}} C_B C_F \sigma_V \quad (3)$$

$$B\cdot\sigma + H_2 \xrightarrow{m_4} P\cdot\sigma + H_2O$$

$$\Rightarrow r_4 = m_4(B\cdot\sigma)C_{H_2} = \frac{m_4}{M_{10}} C_B C_{H_2} \sigma_V \quad (4)$$

$$P\cdot\sigma + F \xleftrightarrow{m_5} R\cdot\sigma \Rightarrow r_5 = m_5(P\cdot\sigma)C_F + m_5'(R\cdot\sigma)$$

$$= \frac{m_5}{M_7} C_P C_F \sigma_v - \frac{m_5'}{M_9} C_R \sigma_V \quad (5)$$

$$N\cdot\sigma \xrightarrow{m_{11}} R\cdot\sigma \Rightarrow r_{11} = m_{11}(N\cdot\sigma) = \frac{m_{11}}{M_8} C_N \sigma_V. \quad (6)$$

2. Homogeneous Reaction Step with Corresponding Rate Equation

$$A \xrightarrow{m_6} F + NM \Rightarrow r_6 = m_6 C_A \quad (7)$$

3. Adsorption/Desorption Steps with Corresponding Equilibrium Relations

$$A + \sigma \xleftrightarrow{M_1} A\cdot\sigma \Rightarrow (A\cdot\sigma) = M_1 C_A \sigma_V \quad (8)$$

$$P\cdot\sigma \xleftrightarrow{M_7} P + \sigma \Rightarrow (P\cdot\sigma) = C_P \sigma_V / M_7 \quad (9)$$

$$N\cdot\sigma \xleftrightarrow{M_8} N + \sigma \Rightarrow (N\cdot\sigma) = C_N \sigma_V / M_8 \quad (10)$$

$$R\cdot\sigma \xleftrightarrow{M_9} R + \sigma \Rightarrow (R\cdot\sigma) = C_R \sigma_V / M_9 \quad (11)$$

$$B\cdot\sigma \xleftrightarrow{M_{10}} B + \sigma \Rightarrow (B\cdot\sigma) = C_B \sigma_V / M_{10}. \quad (12)$$

4. Overall Balance of Catalyst Active-Site Concentrations.

$$\sigma_V + (A\cdot\sigma) + (B\cdot\sigma) + (P\cdot\sigma) + (N\cdot\sigma) + (R\cdot\sigma) = \sigma_t$$

$$\sigma_V = (\sigma_t 1 + M_1 C_A + C_B/M_{10} + C_P/M_7 + C_N/M_8 + C_R/M_9)^{-1}. \quad (13)$$

The preceding rate equations (Eqs. 2–7 on eliminating σ_V using Eq. 13) represent the reaction rates for individual reactions in the network. These could be used to fit the mechanism if enough slurry reaction data were available. Since no measure of the apparent rates is available, this would not be useful for predicting trickle-bed performance. In fact, the only database covering the desired concentration range available is the trickle-bed data. This needs apparent rate forms for species and a reactor model to evaluate the kinetic parameters using reactor outlet concentration data. The reactor model requires the rates of appearance or disappearance of the individual species. These can be directly obtained by linear combination of the preceding rates as follows:

$$-r_A = r_2 + r_6 \quad (14)$$

The intermediate (hydroxyamine) is assumed to have a zero net rate, hence

$$r_B = r_2 - r_3 - r_4 = 0 \quad (15)$$

$$r_N = r_3 - r_{11} \quad (16)$$

$$r_R = r_5 + r_{11} \quad (17)$$

$$r_P = r_4 - r_5 \quad (18)$$

$$r_F = -r_3 - r_5 + r_6 \quad (19)$$

Since these equations contain a very large number of kinetic and equilibrium parameters, some simplifying assumptions need to be made in order to obtain estimates of the most relevant parameter values with the limited amount of experimental data available. The numerator rate and equilibrium constants in Eqs. 2–6 can be lumped into single parameters, and the denominator can be simplified by making the

sumption that the adsorption equilibrium constants are very low ($M_1 \ll 1$ and the desorption equilibrium constants are very high, M_7, M_8, M_9, $M_{10} \gg 1$). This implies (as a first approximation)

$$M_1 C_A + C_B/M_{10} + C_P/M_7 + C_N/M_8 + C_R/M_9 \ll 1. \quad (20)$$

The denominator of Eq. 13 thus reduces to unity in all the preceding rate equations (Eqs. 14–19), and the number of parameters to be fitted is reduced to seven, as shown below. The overall rate equations for individual species (with all parameters lumped in the k values) are then written as,

$$-r_A = k_3 C_A C_{H_2}^2 + k_5 C_A \quad (21)$$

$$r_B = k_3 C_A C_{H_2}^2 - k_4 C_B C_{H_2} - k_2 C_B C_F = 0 \quad (22)$$

$$r_N = k_2 C_B C_F - k_6 C_N \quad (23)$$

$$r_R = k_7 C_P C_F - k_1 C_R + k_6 C_N \quad (24)$$

$$r_P = k_4 C_B C_{H_2} - k_7 C_P C_F + k_1 C_R \quad (25)$$

$$r_F = k_5 C_A - k_2 C_F C_B - k_7 C_F C_P + k_1 C_R. \quad (26)$$

Trickle-bed reactor model

A heterogeneous plug-flow model (El-Hisnawi, 1981; Khadilkar et al., 1996) was used to simulate the trickle-bed reactor. The equations for any liquid-phase component can be written for a liquid reactant limited reaction as

$$-u_{SL}\frac{dC_{i,L}}{dz} - k_{LS}a_{LS}[C_{i,L} - C_{i,LS}] - \Sigma r_{\text{hom }o.} = 0, \quad (27)$$

where

$$k_{LS}a_{LS}(C_{i,L} - C_{i,LS}) = \eta_{CE}\Sigma r_{\text{hetero}}. \quad (28)$$

The equations for the gaseous component present in the liquid phase can be written as

$$-u_{SL}\frac{dC_{j,L}}{dz} + (ka)_{gL}[C_{j,e} - C_{j,L}] - k_{LS}a_{LS}[C_{j,L} - C_{j,LS}] - \Sigma r_{\text{hom }o.} = 0, \quad (29)$$

where

$$k_{LS}a_{LS}(C_{j,L} - C_{j,LS}) = \eta_{CE}\Sigma r_{\text{hetero}}. \quad (30)$$

Inlet conditions for the liquid-phase concentration of the gaseous reactant are $C_{j,L}(z)|_{z=0} = 0$ (nonequilibrium feed), and those for liquid-phase reactant concentration are $C_i(z)|_{z=0} = C_{i0}$

The rates used here are apparent rates (evaluated from the intrinsic rates proposed earlier by assuming a constant pellet effectiveness factor, which is lumped in the rate constants during model fitting). It was assumed here that all reactions are liquid limited for the range of reactant compositions and operating pressures investigated [this assumption is valid for reactant feed concentrations of up to 20% by weight based on the reactant limitation criterion given by Beaudry et al. (1987), and Khadilkar et al. (1996) for simple reactions]. Another simplification was to assume that the external mass-transfer rates were not limiting the overall rate. This was validated on the basis of approximate estimates of the mass-transfer rates using volumetric gas–liquid and liquid–solid mass-transfer coefficients obtained from typical correlations [Tan and Smith (1980) for liquid–solid and Fukushima and Kusaka (1977) for gas–liquid (Figure 2)], and comparing them with the experimentally observed rates of reaction. It was seen for all the experimental data that the observed rate of reaction in the trickle-bed was much lower than the estimated mass-transfer rates. This implies that the liquid-phase concentration can be used directly to calculate apparent rates in the model equations given earlier without significantly affecting the accuracy of the model prediction. The external liquid–solid contacting efficiency was obtained from the correlation of Al-Dahhan and Duduković (1995) and El-Hisnawi (1981). The temperature dependence of the rate parameters was also ignored due to all data sets being acquired at the same inlet and exit temperature and thus reflect the rate data at some intermediate temperature.

Results and Discussion

Global seven-parameter optimization fits were not attempted here since they would require a much larger database and accurate determination and quantification of byproduct species for which the information is currently unavailable.

The model predictions were obtained by choosing three parameters and fitting four of the seven parameters by optimizing an objective function χ^2, which in turn is a function of combination of the experimental and predicted product concentrations:

$$\chi^2 = \sum_{i=1}^{N}\left[\frac{Y_{\text{exp},i} - Y_{fit,i}}{\sigma_i}\right]^2, \quad (31)$$

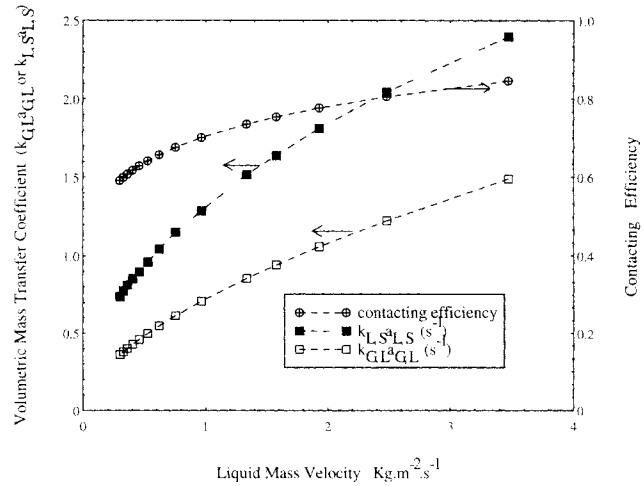

Figure 2. Effect of liquid mass velocity on volumetric mass-transfer coefficients [gas–liquid from Fukushima and Kusaka (1977) and liquid–solid from Tan and Smith (1980)] and contacting efficiency from Al-Dahhan and Duduković (1995) and El-Hisnawi (1981).

Table 2. Reactor Feed and Exit Concentrations for Trickle-Bed Experiments

$C_{NA,feed}$ mol/m^3	$C_{F,feed}$ mol/m^3	$C_{NA,exit}$ mol/m^3	$C_{AA,exit}$ mol/m^3	$C_{F,exit}$ mol/m^3	$C_{NR,exit}$ mol/m^3	$C_{RN,exit}$ mol/m^3
651.0	34.3	0.0	548.0	52.0	19.0	67.0
651.0	34.3	0.0	537.0	25.0	8.0	78.0
651.0	34.3	21.0	418.0	50.0	16.0	138.0
651.0	34.3	23.0	377.0	274.0	17.0	183.0
357.0	19.0	0.0	322.0	0.0	6.0	29.0
357.0	19.0	0.0	243.0	0.0	27.0	87.0
357.0	19.0	0.0	239.0	0.0	9.0	109.0
357.0	19.0	28.0	175.0	0.0	4.0	150.0
1,376.0	72.0	0.0	978.0	182.0	183.0	105.0
1,376.0	72.0	0.0	817.0	115.0	142.0	375.0
1,376.0	72.0	0.0	666.0	490.0	38.0	254.0
1,896.0	99.0	59.0	1,117.0	42.0	256.0	564.0
1,896.0	99.0	68.0	1,052.0	279.0	344.0	254.0
1,896.0	99.0	119.0	935.0	356.0	248.0	358.0
890.0	47.0	0.0	550.0	37.0	76.0	181.0
890.0	47.0	0.0	492.0	29.0	74.0	248.0
890.0	47.0	0.0	425.0	25.0	12.0	292.0
890.0	47.0	0.0	316.0	40.0	9.0	399.0
477.0	25.0	0.0	411.0	0.0	9.0	81.0
477.0	25.0	0.0	396.0	0.0	10.0	97.0
477.0	25.0	0.0	324.0	0.0	15.0	163.0
477.0	25.0	0.0	301.0	0.0	25.0	176.0

where σ_i is the standard deviation in experimental data point $Y_{exp,i}$.

The objective function for the fitting can be set to be the individual species concentrations independently for all the reaction runs, and the entire concentration data set (Table 2) could be assigned equal weight. However, the degree of accuracy in determining individual byproduct concentrations is not as high as for the main product concentration, which is known accurately due to the use of internal standardization and accurate gas chromatograph calibration with pure product (aminoalcohol). Hence, an objective function was chosen by assigning a higher weight to the product concentration as compared to byproduct concentrations, which are assigned weights α, β, and γ corresponding to furfural, nitrone, and reduced nitrone concentration, respectively.

$$Y_{fit} = (C_P + \alpha C_F + \beta C_{NR} + \gamma C_{RN})_{pred} \quad (32)$$

$$Y_{exp} = (C_P + \alpha C_F + \beta C_{NR} + \gamma C_{RN})_{exp}. \quad (33)$$

The Levenberg–Marquardt algorithm (Press et al., 1992) was used to optimize the chosen parameters based on nonlinear least-squares fitting of the experimental data. The gradient vector of the objective function with respect to the parameters was calculated numerically and supplied along with the objective function evaluation. Model predictions were found to be more sensitive to the values of parameter k_3, k_5, and k_7 than to other parameters. Model predictions were obtained using assumed values of k_1, k_6, and k_7 and fitted values of k_2, k_3, k_4, k_5 for Set I, while for Set II k_3, k_4, and k_7 were assigned values and the rest were fitted by the optimization program. They were seen to give reasonably good fits of the desired product composition, but do not fit byproduct concentrations well. This is due to the higher weight assigned to the desired product concentration as compared to byproduct concentrations. Comparison of the reactor-model predicted (with the fitted rate constants) values of the desired product concentration with the experimental values for the entire data set is shown in Figure 3 (for parameter Set I). The predicted variation of the product composition with liquid mass velocity for selected values of feed compositions is shown in Figure 4 for parameter Set I to illustrate that the flow dependence of the experimental concentration profile of product is captured by the fitted values. The values of rate parameters obtained for corresponding byproduct concentration weighting factors are listed in Table 3. The AAREs for fitted concentrations are less than 15% in both sets. These are not the globally optimum values of k, as some of the k's were held at preassigned values. Nevetheless, the primary objective of demonstrating the feasibility and usefulness of this approach as a tool in kinetic analysis and reactor design for

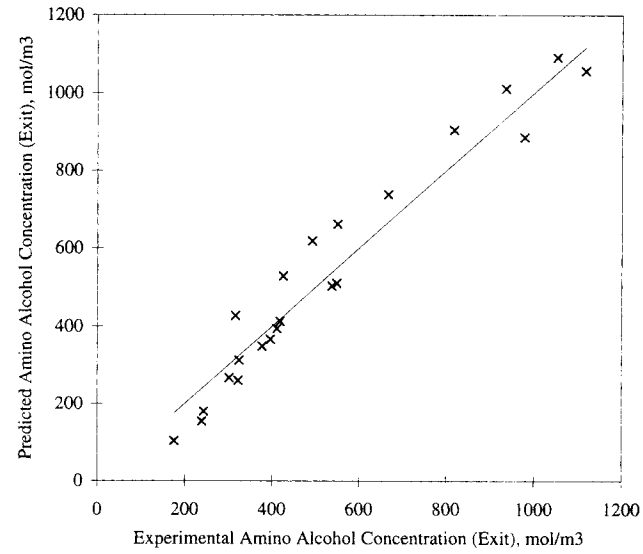

Figure 3. Predicted vs. experimental AA concentrations using the fitted parameter Set I.

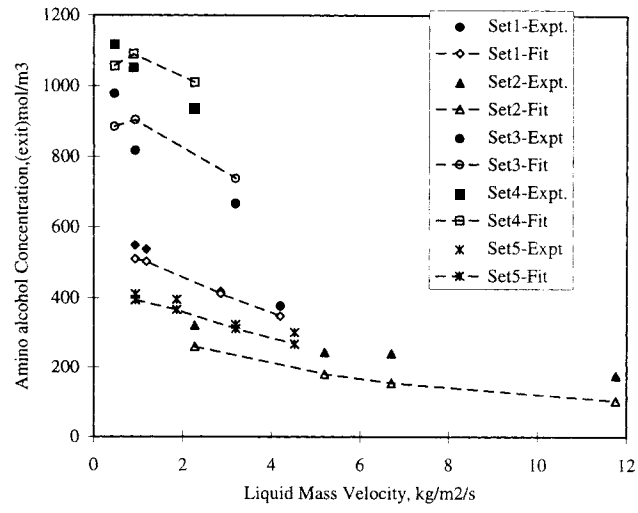

Figure 4. Effect of liquid mass velocity on predicted (Set I) and experimental concentration of AA.

Table 3. Byproduct Weighting Factors and Rate Parameters

Concentration Weighting Factors	Assigned Kinetic Parameters	Fitted Kinetic Parameters
Set I	$k_1 = 3.0\times10^{-8}$	$k_2 = 1.08\times10^{-3}$
$\alpha = 0.1;\ \beta = 0.2\ \gamma = 0.2$	$k_6 = 8.0\times10^{-7}$	$k_3 = 1.94\times10^{-5}$
	$k_7 = 1.0\times10^{-5}$	$k_4 = 2.5\times10^{-4}$
		$k_5 = 7.97\times10^{-7}$
Set II	$k_3 = 1.95\times10^{-5}$	$k_1 = 4.37\times10^{-9}$
$\alpha = 0.1;\ \beta = 0.1;\ \gamma = 0.8$	$k_4 = 2.15\times10^{-4}$	$k_2 = 9.98\times10^{-6}$
	$k_7 = 1.0\times10^{-5}$	$k_5 = 6.39\times10^{-7}$
		$k_6 = 8.1\times10^{-7}$

Units of k's are consistent with Eqs. 21–26 when concentration is expressed in mol/m^3 and time in seconds.

complex reaction systems has been achieved in the present study.

Conclusions

A kinetic scheme for a complicated reaction network was developed on the basis of the mechanism proposed in this article. Based on a trickle-bed reactor model and parameter-optimization programs, it was possible to obtain the approximate kinetic constants using the experimental data acquired in the trickle-bed experiments that were otherwise unobtainable using conventional slurry and basket reaction tests. Although the predictions show promise, more experimental data are needed if all the parameters have to be successfully fitted to the entire data set. An optimization based on bounded values of the parameters is necessary to get realistic optimum parameter values for all the k's. Such kinetic model development is important for performance evaluation, optimization, and scale-up to commercial reactor for this and similar complex reaction schemes.

Acknowledgment

The financial support of the Agricultural Research Center at the Monsanto Company in St. Louis, Missouri, is gratefully acknowledged.

Notation

a_{LS} = liquid–solid contact area per unit reactor volume
a_{GL} = gas–liquid contact area per unit reactor volume
AARE = average absolute relative errors
C_A = concentration of nitroalcohol, mol/m^3
$C_{A,0}$ = feed concentration, mol/m^3
C_B = concentration of hydroxyamine, mol/m^3
$C_{F,0}$ = concentration of furfural in feed reactant mixture, mol/m^3
C_N = concentration of nitrone, mol/m^3
C_P = concentration of aminoalcohol (product), mol/m^3
C_R = concentration of reduced nitrone, mol/m^3
$C_{j,e}$ = equilibrium concentration of gaseous reactant in the liquid phase, mol/m^3
$C_{i,L}/C_{j,L}$ = concentration of species i or j in liquid phase, mol/m^3
$C_{j,LS}$ = concentration of gaseous reactant in the liquid phase on the catalyst surface, mol/m^3
k_i = rate constant of reaction
$= \frac{m'_5}{M_9}\sigma_V;\ k_2 = \frac{m_3}{M_{10}}\sigma_V;\ k_3 = m_2 M_1 \sigma_V;\ k_4 = \frac{m_4}{M_{10}}\sigma_V;\ k_5$
$= m_6;\ k_6 = \frac{m_{11}}{M_8}\sigma_V;\ k_7 = \frac{m_5}{M_7}\sigma_V$
k_{LS} = liquid–solid mass-transfer coefficient, m/s
k_{GL} = gas–liquid mass-transfer coefficient, m/s
m_j = rate constant of surface reaction ($j = 2, 3, 4, 5, 6, 11$)
M = mass of catalyst, kg
M_j = equilibrium constant of adsorption or desorption ($j = 1, 7, 8, 9, 10$)
r_{hetero} = heterogeneous reaction rate, mol/m^3·s
r_{homo} = homogeneous reaction rate, mol/m^3·s
r_i = reaction rate based on component i (i = A, B, N, R, F, P)
r_j = reaction rate based on the surface reaction step ($j = 2, 3, 4, 5, 6, 11$)
t = reaction time, s
u_{SL} = liquid superficial velocity, m/s
Y_{fit} = objective function, predicted
Y_{exp} = objective function, experimental
z = axial coordinate in the reactor, m
σ_i = variance in Y_{exp}
σ_V = concentration of vacant active sites on the surface of catalyst as shown in Eq. 13
η_{CE} = external liquid–solid contacting efficiency
χ = minimization function for data fitting

Literature Cited

Al-Dahhan, M., and M. P. Duduković, "Catalyst Wetting Efficiency in Trickle-Bed Reactors at High Pressure," *Chem. Eng. Sci.*, **50**, 15, 2377 (1995).

Beaudry, E. G., M. P. Duduković, and P. L. Mills, "Trickle Bed Reactors: Liquid Diffusional Effects in a Gas Limited Reaction," *AIChE J.*, **33**(9), 1435 (1987).

El-Hisnawi, A. A., "Tracer and Reaction Studies in Trickle-Bed Reactors," DSc Thesis, Washington Univ., St. Louis, MO (1981).

Fukushima, S., and K. Kusaka, "Liquid-Phase Volumetric Mass Transfer Coefficient and Boundary of Hydrodynamic Flow Region in Packed Column with Cocurrent Downward Flow," *J. Chem. Eng.*, Jpn, **10**, 468 (1977).

Khadilkar, M. R., Y. Wu, M. H. Al-Dahhan, M. P. Dudukovic, and M. Colakyan, "Comparison of Trickle-Bed and Upflow Performance at High Pressure: Model Predictions and Experimental Observations," *Chem. Eng. Sci.*, **51**(10), 2139 (1996).

Press, W. H., S. A. Teukolsky, W. T. Vetterling, and B. P. Flannery, *Numerical Recipes in FORTRAN*, Cambridge Univ. Press, New York (1992).

Tan, C. S., and J. M. Smith, "Catalyst Particle Effectiveness with Unsymmetrical Boundary Conditions," *Chem. Eng. Sci.*, **35**, 1601 (1980).

Manuscript received Sept. 22, 1997, and received Jan. 20, 1998.